Applied Clay Science 132–133 (2016) 600–610

Contents lists available at ScienceDirect

Applied Clay Science

journal homepage: www.elsevier.com/locate/clay

Research paper

Crystallographic, vibrational, thermal and electrochemical properties of nacrite-NH_4Cl nanohybrid

Nouha Jaafar *, Hafsia Ben Rhaiem, Abdesslem Ben Haj Amara

UR13ES46: Unity of Research of Physics of Lamellar Materials and Hybrid Nano-Materials, University of Carthage, Faculty of Sciences of Bizerte, Zarzouna 7021, Tunisia

ARTICLE INFO

Article history:
Received 24 June 2016
Received in revised form 7 August 2016
Accepted 8 August 2016
Available online 11 August 2016

Keywords:
Layered material
Clay mineral
Nanohybrid
Intercalation reaction
X-ray diffraction
Ionic conductivity

ABSTRACT

$Si_2Al_2O_5(OH)_4 \cdot (1-\chi)NH_4Cl \cdot (1-\chi)H_2O$ nanohybrid was prepared by indirect intercalation of ammonium chloride into the interlamellar space of nacrite. The number and position of intercalated ions and water molecules, the layer thicknesses, the stacking mode along the normal to the layer plane (z) were determined by modelling X-ray diffraction patterns. Infrared spectroscopy was carried out to observe the interactions between the silicate "network" and the ammonium chloride salt. Thermogravimetric analysis was achieved to study the phase transition of the nanohybrid when the system temperature is increased. Finally, the electrochemical identification of the new nanohybrid material was performed with both parameters: frequency and temperature. Indeed, the prepared compound has a fairly high ionic conductivity at higher temperatures and can be classified as a superionic conductor.

1. Introduction

Clays and clay minerals are interesting materials not only because of their low cost but also because they are ubiquitous and environment friendly (Bergaya and Lagaly, 2006; Zhou and Keeling, 2013). Moreover, clay minerals are at the epicenter of nanohybrid lamellar materials research (Fernandes et al., 2014).

It is well-documented that the surface and the interlayer space of clay minerals can be modified. Furthermore, the interlayer space of clay minerals can also act as a confined nanoreactor for in situ interlayer reaction and a nanoscale 'container' for confined nucleation, growth, or clustering of nanoparticles and nanoaggregate (Zhou et al., 2016). Intercalation is probably the most often used method for modifying clay minerals (Zhu et al., 2014). Intercalated clay minerals, have found wide applications in environmental remediation, e.g., as adsorbents for inorganic and organic contaminants, and catalysts for the degradation of organic contaminants. Intercalated clay minerals have also been used as a carrier for drugs, pesticides, and biochemicals for various application purposes (Zhu et al., 2014). The capability of tuning materials' performances, not only in terms of tailoring their physico-chemical properties to answer prerequisites of a given application, but also regarding the elaboration of novel concepts, opened a door to a radical new world in materials science (Fernandes et al., 2014).

Kaolin is one of the naturally occurring abundant clays in the earth's crust. The kaolin group consists of dioctahedral 1:1 layer structures with the idealized formulae $Si_2Al_2O_5(OH)_4$. Dehydrated kaolin minerals shows different polytypes: kaolinite, dickite and nacrite and halloysite-(0.7 nm) (Brigatti et al., 2013). These clay minerals are characterized by certain properties, including a layer structure with one dimension in the nanometer range, the thickness of this 1:1 layer is about 0.7 nm (Bergaya and Lagaly, 2006). One side of the layer is gibbsite-like with aluminum atoms octahedrally coordinated to corner oxygen atoms and hydroxyl groups. The other side of the layer constitutes a silica-like structure in which the silicon atoms are tetrahedrally coordinated to oxygen atoms. The adjacent layers are linked via hydrogen bonds (O—H···O) involving aluminol (Al—OH) and siloxane (Si—O) groups (Wypych and Satyanarayana, 2004).

From the initial pioneering works to nowadays, a great number of contributions have been published dealing with the intercalation of organic and/or inorganic guest species between the layers of kaolinite forming nanohybrid materials (Brunet et al., 2015).

In the same line, the extensive study of Tunisian nacrite (Table 1), as mentioned in the bibliometric data (Ben Haj Amara et al., 1998, 2000; Naamen et al., 2004; Jaafar et al., 2014, 2015, 2016), illustrates that this layered clay mineral has high chemical stability and well-packed structure which constitute a suitable host matrix for the incorporation of inorganic salts (LiCl (Jaafar et al., 2016), CsCl (Naamen et al., 2004), KCl (Naamen et al., 2004), and $MgCl_2 \cdot 6H_2O$ (Jaafar et al., 2014)) or organic compounds such as (DMSO, NMA) (Ben Haj Amara et al., 2000). The intercalation of organic and/or inorganic guest species in the

* Corresponding author.
E-mail address: nouhajaafar@yahoo.fr (N. Jaafar).

http://dx.doi.org/10.1016/j.clay.2016.08.010
0169-1317/

Table 1
Crystallographic data of a well-crystallized Tunisian nacrite (Ben Haj Amara et al., 1998).

Chemical formula	$Si_2Al_2O_5(OH)_4$
Crystal system	Monoclinic
Space group	Cc
Stacking mode	2 M
Cell parameters	$a = 0.8906$ nm
	$b = 0.5146$ nm
	$c = 1.5669$ nm
	$\beta = 113.58°$
Basal spacing	$d_{002} = c \sin\beta/2 \cong 0.72$ nm

interlayer space of nacrite has shown the importance of preparing new nanohybrid materials with both structural and functional properties.

In order to throw some additional light on the role of cation (nature, charge and location) on the expansion of Tunisian nacrite, this research was broadened to prepare a new nanohybrid material via intercalation of nacrite with a polyatomic cation: NH_4^+. Noteworthy, the intercalation of NH_4Cl into the interlayer space of kaolinite failed in the major previous experiments. However, ammonium chloride was smoothly adsorbed (Wada, 1959) or directly sandwiched (Garrett and Walker, 1959) within the interlayer region of halloysite.

An innovative and inexpensive experimental hybridization process has been adopted to ensure the synthesis of nacrite-NH_4Cl nanohybrid material. The elaborated nanohybrid exhibited significantly improved crystallographic, vibrational and electrical characteristics compared to that of unmodified nacrite. Furthermore, the in-situ heat treatment of the nanohybrid, the phase transition and its influence on the conduction has been comprehensively undertaken in the present work. The ultimate goal of this paper was to reflect upon all these characterizations, how this new nanohybrid with improved functionality could be integrated from a technologic point of view.

2. Materials and methods

2.1. Materials

The raw nacrite used was collected from North Tunisia (Ben Haj Amara et al., 1998, 2000) (mine of Jbel Slata, Kef). This starting clay material shows large particles with minor impurities. Potassium acetate (CH_3COOK) and ammonium chloride (NH_4Cl) were purchased from Prolabo. The purities of all chemicals were >99%.

2.2. Nanohybrid preparation

The intercalation of ammonium chloride salt into the interlayer space of nacrite was carried out indirectly by means of an entraining agent, i.e., potassium acetate. Potassium acetate "KAc" was the best precursor selected for the expansion of nacrite. In fact, KAc was widely used as a small and highly polar molecule for the intercalation of guest species that could not directly intercalate kaolin materials (Ben Haj Amara et al., 2000).

It was then possible to prepare nacrite-NH_4Cl nanohybrid material in two steps: The first step, has been already detailed and published in the previous research papers (Ben Haj Amara, 1997; Ben Haj Amara et al., 1998) where the raw nacrite ($d_{002} = 0.72$ nm) was converted into nacrite-KAc complex ($d_{002} = 1.40$ nm) (Fig. 1). The CH_3COOK was then successfully eliminated by repeated washing of the nacrite-KAc intercalate with deionized water and air-drying until the elaboration of a homogeneous hydrate ($d_{002} = 0.84$ nm) (Fig. 1). Removal of the intercalated CH_3COOK was proofed by referring to the vibrational characterization of hydrated nacrite (Ben Haj Amara, 1997; Jaafar et al., 2015). Analysis of the features and assignment of infrared (IR) bands provide the significant differences and the obvious structural change between the nacrite-KAc complex and the hydrate (Jaafar et al., 2015). The disappearance of C═O antisymmetric stretching vibration around 1572 cm^{-1}; O—C—O symmetric stretching vibration around 1423 cm^{-1} and the symmetric deformation band of the CH_3 group around 1351 cm^{-1} (Jaafar et al., 2015), and, meanwhile the perturbations in both the position and the intensity of the hydroxyl vibration modes in the IR spectrum of the hydrate gave evidence of the removal of acetate and potassium ions (Jaafar et al., 2015; Zhang et al., 2011).

In the second step, 4.81 g of NH_4Cl dissolved in water (Normality = 3 N) was added to the hydrate. The mixture was then heated at 50 °C under a magnetic stirring for 7 days. The resulting complex was kept at ambient atmosphere for three hours. The use of water as solvent favor the expansion of the clay mineral and the intercalation of the ammonium chloride within the nacrite layers leading to the resulting nacrite-NH_4Cl nanohybrid ($d_{002} = 1.03$ nm) (see Fig. 1).

2.3. Characterization techniques

X-ray diffraction (XRD) pattern of nacrite-NH_4Cl nanohybrid was performed at ambient temperature using a reflection setting on a Bruker D8 installation monitored by the EVA-version Diffrac plus software (Bruker AXS GmbH, Karlsruhe, Germany) and $CuK\alpha_1$ radiation. Usual scanning parameters were 0.02°2θ as step size and 6 s as counting time per step over the angular range 5–120°2θ.

IR spectra were recorded at ambient temperature using a thermo scientific Nicolet IR 200 FT-IR with ATR Spectrometer, equipped with a diamond crystal and operating in the medium IR [4000–400 cm^{-1}] spectral region. IR spectroscopy was used as a reliable tool for the characterization of intercalation nanohybrids in order to examine the interactions between functional surface groups of the nacrite layers and the ammonium chloride.

Thermogravimetric analysis (TGA) of nacrite-NH_4Cl nanohybrid was carried out using a 92 SETARAM equipment in flowing air, in a temperature ranging from ambient temperature to 800 °C along with a heating rate of 5 °C/min. This technique was very powerful to monitor the structural modification of clay minerals when heated at different temperatures.

Electrochemical Impedance Spectra (EIS) were performed using a frequency response analyzer (Hewlett-Packard 4192). Complex impedance measurements were performed in an open circuit using two electrode configurations with signal amplitude of 50 mV and a frequency band ranging from 10 Hz to 13 MHz at different temperatures. The examined sample was pressed into pellet using a hydraulic press. To ensure good electrical contact between the sample and the electrical junctions, the pellet was sandwiched between two platinum electrodes to form a symmetrical cell. The cell was eventually placed into a programmable oven coupled with a temperature controller. The collected data were fitted using the equivalent circuit of the *Zview* software.

3. Results and discussion

3.1. Diffraction data collection and refinement

3.1.1. Qualitative XRD analysis

Examining the experimental 00*l* reflections of the stable nacrite-NH_4Cl nanohybrid, (Fig. 2), a main 00*l* reflection at $2\theta_{002} = 8.570°$ and $d_{002} = 1.03 \pm 0.002$ nm basal spacing value can be observed. This means that an expansion of the interlayer space of nacrite by ~0.31 nm along the c^* axis has occurred. This result is probably due to the insertion of ammonium chloride salt with one water sheet into the nacrite matrix. Additional reflections are attributed to excess of salt and are identified by (°) symbol.

Data in Table 2 reveals that the number of layers per particle, $\overline{M}$, deduced from the classic Debye-Scherrer formula (Eq. (1)) decreases from "$\overline{M} = 70 \pm 1$" for raw nacrite (Ben Haj Amara et al., 1998) to "$\overline{M} = 17 \pm$

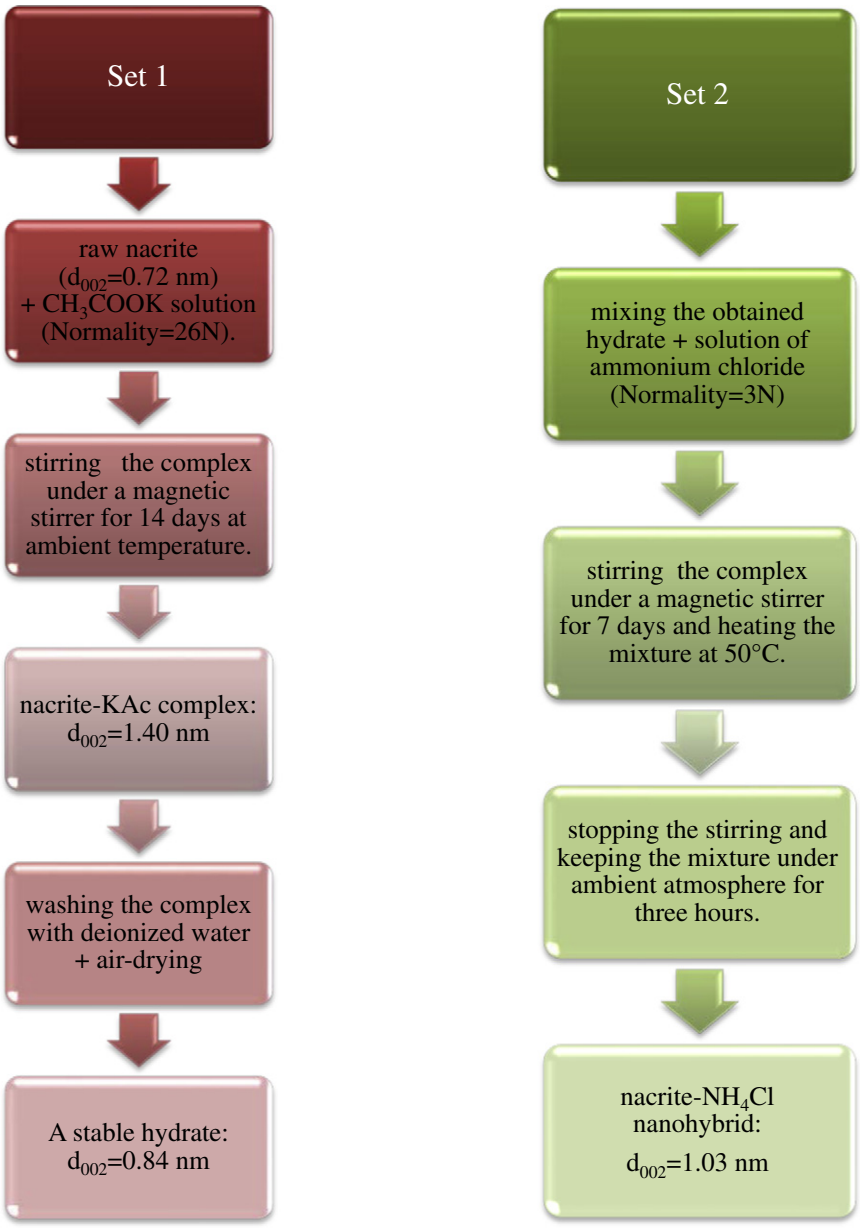

Fig. 1. Summary of the experimental protocol to synthesize nacrite-NH_4Cl nanohybrid. Note: the first set is previously studied and detailed by Ben Haj Amara et al. (2000).

1" for nacrite-NH_4Cl nanohybrid.

$$\overline{M} = \frac{K\,\lambda}{l\,d_{00l}\cdot FWHM\left(\text{Å}2\theta\right)\cdot cos\theta_{00l}} \quad (1)$$

where K is the Scherrer constant equal to 0.886, λ is the wavelength used, (ld_{00l}) the apparent distance deduced from the maximum intensity for all measurable 00l reflections and FWHM (°2θ) represents the angular width at half-height of 00l reflections.

This result can be ascribed to particle cleavage and break of coherence during the intercalation process.

The degree of reaction is calculated from the intensities of the 00l reflections of the untreated nacrite, I_N, and the intercalation compound, I_I (Lagaly et al., 2006):

$$\alpha = \frac{I_I}{I_N + I_I} \quad (2)$$

The degree of reaction is equal to 0.94 for nacrite-NH_4Cl nanohybrid. Accordingly, the intercalation process of nacrite with ammonium chloride is practically complete.

3.1.2. Quantitative XRD analysis

Quantitative analysis requires an XRD-modelling computer program: theoretical XRD patterns are then reproduced to fit the experimental one related to nacrite-NH_4Cl nanohybrid. The theoretical intensities are calculated from the matrix expression developed by Drits and Tchoubar (1990):

$$I_{00}(2\theta) = L_p\ \ Spur\left(Re\,[\Phi][W]\left\{[I] + 2\sum_{n}^{M-1}\frac{M-n}{M}[Q]^n\right\}\right) \quad (3)$$

where Re signifies the real part of the final matrix; Spur, the sum of the diagonal terms of the real matrix; L_p, the Lorentz-polarization and absorption factor; M, the number of layers per stacking; n, an integer varying between 1 and M-1; [Φ], the structure factor matrix; [I],the unit

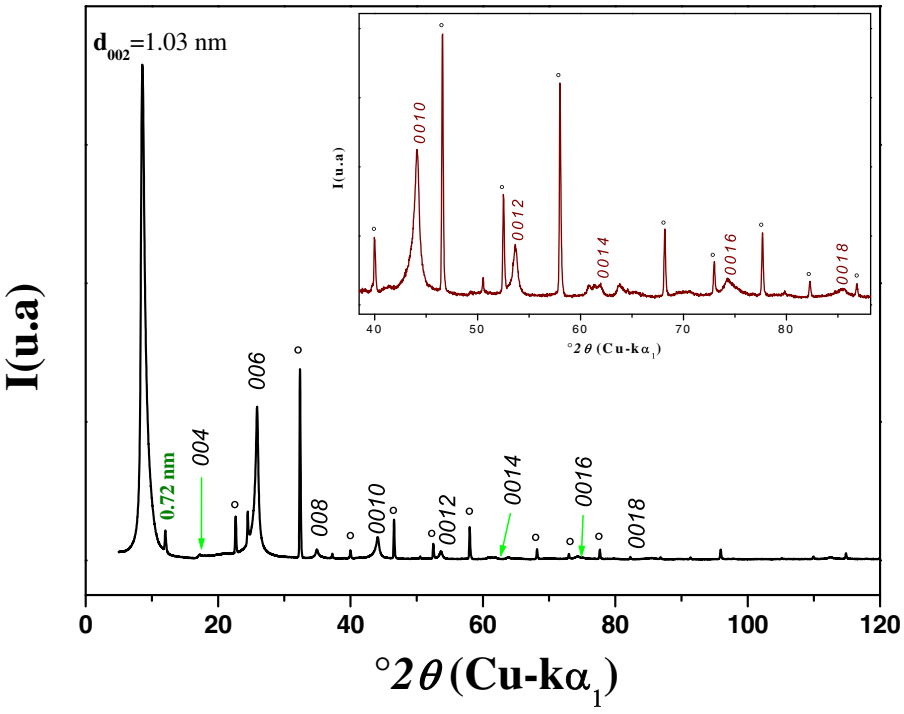

Fig. 2. Experimental XRD pattern of the nacrite-NH_4Cl nanohybrid. °: reflections related to the excess of the salt: [Data Base PDF2: 01-089-2787. Compound name: ammonium chloride. Formula NH_4Cl].

matrix; [W], the diagonal matrix of the proportions of the different kinds of layers, and $[Q]^n$, the matrix representing the interference phenomena between adjacent layers. This formalism allows the determination of the mean number of layers per stacking, the abundances W_i of the different kinds of layers and the succession law of the layers within the stacking P_{ij}, P_{ij} is the probability of passing from a *i* layer to a *j* one.

The reliability factor, R_p, plays an important role in judging model adequacy (Taser et al., 1997):

$$R_p = \sqrt{\frac{\sum\left[I(2\theta_i)_{obs} - I(2\theta_i)_{calc}\right]^2}{\sqrt{\left[I(2\theta_i)_{obs}\right]^2}}} \quad (4)$$

where, $I(2\theta_i)_{obs}$ and $I(2\theta_i)_{calc}$ represent the measured and calculated intensities, respectively, at the $2\theta_i$ position, the subscript *i* running over all points in the refined angular range. The best agreement between the observed and calculated patterns corresponds to the lower values of R_p.

On the basis of these modelling data, the following structural parameters: the abundance, the probabilities and number of layers per stacking, the number and position of the intercalated species and water molecules along the ***z*** axis are deduced.

The adequate fit between the experimental and theoretical XRD patterns of the nacrite-NH_4Cl nanohybrid (Fig. 3) is obtained according to both intensity and profile with a reliability factor ($R_p = 7.28\%$). This agreement corresponds to the following structural parameters per half unit-cell: one NH_4^+ cation located at $\boldsymbol{z} = 0.81 \pm 0.01$ nm, one Cl^- anion located at $\boldsymbol{z} = 0.66 \pm 0.01$ nm and one H_2O molecule situated at $\boldsymbol{z} = 0.70 \pm 0.01$ nm and sandwiched between the cation and the anion (Table 3). The origin of the ***z*** coordinates was taken at the basal oxygen atoms along the normal to the layer. This model suggests the presence of a hydrated salt. A structural configuration is given in Fig. 4.

In summary, the intercalated cations are located close to the ditrigonal holes of the tetrahedral sheet, whereas the intercalated anions are located close to the inner-surface hydroxyls of the octahedral sheet of the subsequent layer.

On the other hand and by referring to previous works (Drits and Tchoubar, 1990; Ben Rhaiem et al., 2000), quantitative analysis of the nacrite-NH_4Cl nanohybrid induced an interstratified stacking mode characterized by a segregation tendency consisting of a total demixion of two types of layers: Layer *A* corresponds to a major fraction ($W_A = 0.94$) of the intercalated nacrite ($d_{002} = 1.03$ nm) and Layer *B* corresponds to a minor layer proportion($W_B = 0.06$) of the non-intercalated nacrite ($d_{002} = 0.720$ nm). The conditional probabilities P_{ij} of passing from layer *i* to layer *j* are $P_{AA} = 1$, $P_{AB} = 0$, $P_{BA} = 0$, $P_{BB} = 1$.

Consequently, the chemical formula of nacrite-NH_4Cl nanohybrid by half-unit cell obtained at ambient temperature was deduced from the XRD results (Table 3):

$$\{(1-\chi)\{Si_2Al_2O_5(OH)_4 \cdot NH_4Cl \cdot 1H_2O\} + \chi\{Si_2Al_2O_5(OH)_4\}\} = \{Si_2Al_2O_5(OH)_4 \cdot (1-\chi)NH_4Cl \cdot (1-\chi)H_2O\}$$

where $\langle\langle\chi = 0.06\rangle\rangle$ corresponds to the non-expanded fraction of nacrite clay mineral.

The number of layers per particle is around 18 ± 1 and is in concordance with the qualitative analysis.

Briefly, comparing these experiment results with the current results of Jaafar et al. (2015) implied that the main basal spacing value of nacrite-NH_4Cl nanohybrid ($d_{002} = 1.03$ nm) is lower than that corresponding to nacrite-LiCl nanohybrid ($d_{002} = 1.14$ nm). Namely, the basal spacing is inversely proportional to the ionic radius of the intercalated cation.

Table 2
Principal qualitative XRD results of nacrite-NH_4Cl nanohybrid.

00*l* reflections	*002*	*004*	*006*	*008*	*0010*	*0012*
I_{002}/I_{00l}	1	84.3	3.20	39.16	20.32	55.97
$(l * d_{00l})_{app}$	10.30	10.40	10.29	10.24	10.25	10.20
FWHM(°2θ)	0.696	0.623	0.464	0.456	0.554	0.453
$\overline{M}$	17					

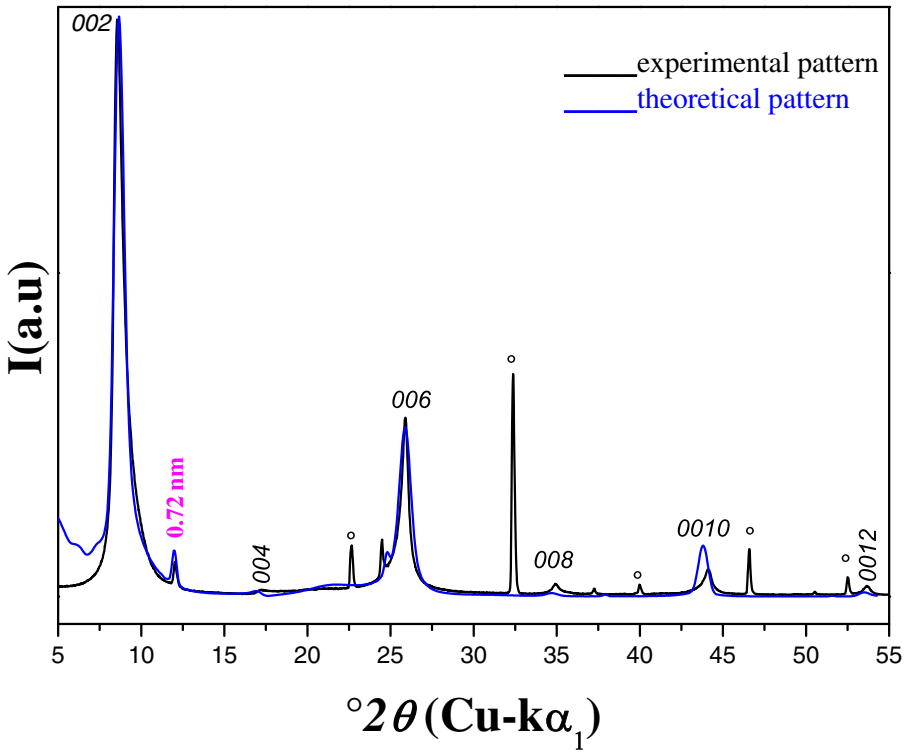

Fig. 3. Best agreement between experimental and theoretical profile of the nacrite-NH_4Cl nanohybrid material.

3.2. Infrared spectroscopy

The IR spectrum of nacrite-NH_4Cl nanohybrid (Fig. 5) revealed modifications in the stretching and deformation vibrations compared to that of untreated nacrite (Jaafar et al., 2016). These changes are due to the intercalation of guest species accompanied with hydration (Yariv et al., 1999) and are detailed as follows:

i) The appearance of NH stretching and deformation vibrations confirmed the keying of NH_4^+ cation.
ii) The appearance of HOH stretching and bending vibrations at 3579 cm^{-1} and 1667 cm^{-1}, respectively, accompanied by shoulders towards lower wavenumbers confirmed the existence of intercalated H_2O molecule as determined by XRD analysis. According to (Frost et al., 2000; Shoval et al., 2001), the intercalated water molecule is bound to both ions of the salt: The cation is bound to the H_2O oxygen by an ion-dipole electrostatic interaction whereas the anion is bound through a hydrogen bond where the water molecule acts as a proton donor as follows: $NH_4\cdots O(H)—H\cdots Cl$.
iii) The weakening of Al—OH stretching vibrations and the slight shifts of Al—O deformation vibrations to higher frequencies is caused by the fact that the inner-surface hydroxyls of the gibbsite sheet are engaged in hydrogen bonds by donating protons to the halide anion: $O—H\cdots Cl^-$. It is important to note that the hydrogen bonds formed between the chlorides and the inner surface OH groups are much stronger than those between the chlorides and the inner OH groups (Yariv et al., 1999).
iv) The Si—O bands are not expected to be affected by intercalation of ammonium chloride into the interlamellar space of nacrite. Indeed, the Si—O stretching vibrations ν(Si—O) shift to lower wavenumbers and the Si—O deformation vibrations δ(Si—O) shift to higher wavenumbers. This phenomenon is attributed to the formation of electrostatic interaction between the ammonium cation and the basal oxygen of the siloxane sheet.

Thus, IR spectroscopy revealed that the incorporated ammonium chloride overcomes the strong interactions between the nacrite-like lamellae to form:

1) hydrogen-bonding between Cl^- anion with the inner-surface hydroxyls of the octahedral sheet.
2) electrostatic interactions between NH_4^+ cation and the negatively charged oxygen of the inner-surface oxygen of the tetrahedral sheet.

Regarding the intercalated H_2O molecule only interacts with the Cl^- and NH_4^+ ions.

Furthermore, the IR spectroscopy determined the localization of the ammonium ion within the interlamellar space of nacrite and therefore identifying its symmetry classification (crystallographic point group).

According to the literature data, an isolated NH_4^+ cation belongs to the symmetry group T_d (tetrahedral – 43 m Hermann Mauguin notation

Table 3
Principal quantitative XRD results of nacrite-NH_4Cl nanohybrid.

Nanohybrid	d_{002} (phase A) (±0.002 nm)	W_A	d_{002} (phase B) (±0.002 nm)	W_B	Proportions	$\overline{M}$ ± 0.01	n_{H2O}	Z_{H2O} (±0.01 nm)	n	Z (±0.01 nm)
Nacrite-NH_4Cl	1.03	0.94	0.72	0.06	$P_{AA} = 1$ $P_{AB} = 0$ $P_{BA} = 0$ $P_{BB} = 1$	18	1	0.70	$n(NH_4^+) = 1$ $n(Cl^-) = 1$	$z(NH_4^+) = 0.81$ $z(Cl^-) = 0.66$

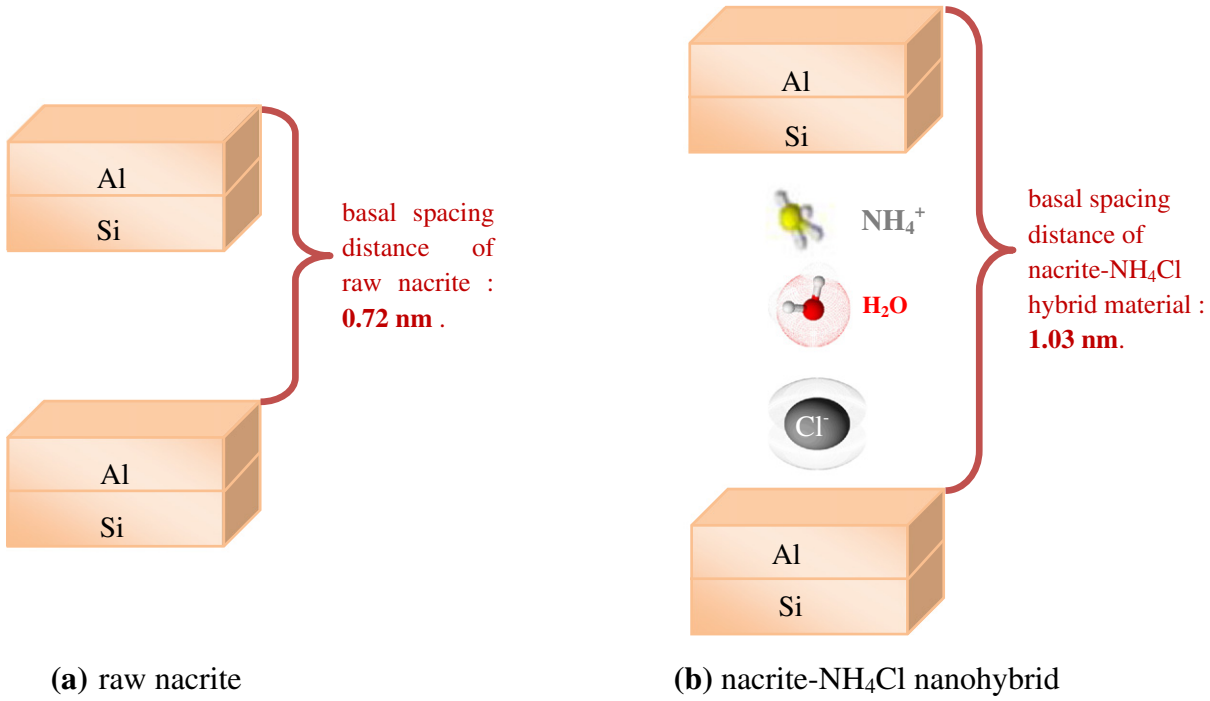

Fig. 4. Schematic representation of (a) raw nacrite, (b) nacrite-NH_4Cl nanohybrid.

equivalent) (Petit et al., 2006). In accordance with the selection rules, the IR spectrum of NH_4^+ ion in a symmetrical environment is characterized by two intense absorption bands at 3150 cm^{-1} and 1400 cm^{-1} and two extra attributed to interactions between these fundamental vibrations at 3040 and 2810 cm^{-1} (Petit et al., 2006). In the case of a structural distortion along one privileged axis of NH_4^+, a loss of the T_d symmetry is brought. A change from T_d symmetry for isolated NH_4^+ ion to C_{3v} (trigonal-3 m notation equivalent) or C_{2v} (orthorombic-2 mm notation equivalent) symmetry is suggested (Petit et al., 2006).

The vibrational spectrum of NH_4^+ ions incorporated in the interlayer space of nacrite observed in Fig. 6 exhibits distinct band positions in comparison to the spectrum of NH_4^+ in a symmetrical environment. It follows then that the T_d symmetry of the NH_4^+ is not maintained. The lower symmetry of adsorbed NH_4^+ is attributed to hydrogen bonding between NH_4^+ and water and/or surface sites on the clay mineral (Petit et al., 2006). Finally, it can be evidenced that ammonium ions are located near to tetrahedral sites of nacrite with a lower symmetry.

3.3. Thermogravimetric analysis

Assessment of thermogravimetric curve illustrates that nacrite-NH_4Cl nanohybrid material $\{Si_2Al_2O_5(OH)_4 \cdot (1-\chi)NH_4Cl \cdot (1-\chi)H_2O\}$

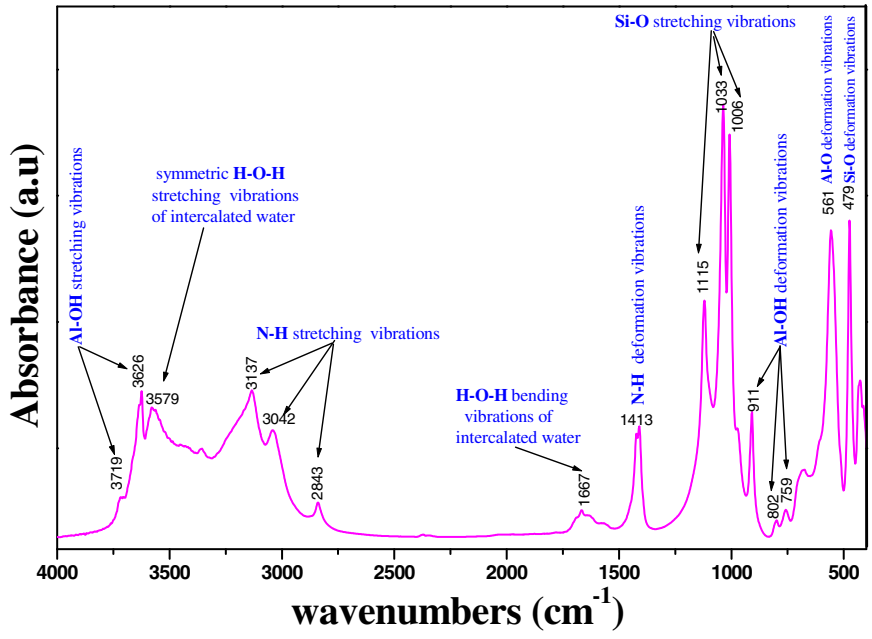

Fig. 5. Wavenumbers and assignments of the IR absorption bands in the 4000–400 cm^{-1} spectral region for the nacrite-NH_4Cl nanohybrid.

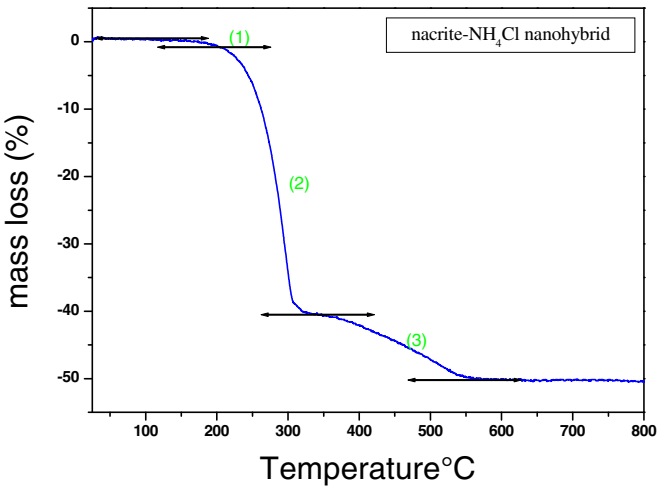

Fig. 6. The TG curves of the nacrite-NH_4Cl nanohybrid heated from room temperature to 800 °C.

loses mass gradually from ambient temperature to 800 °C as shown in Fig. 6 and Table 4. The first mass loss, detected between 25 and 150 °C corresponds to the removal of intercalated water molecule and confirms the XRD results. The structural composition becomes $\{Si_2Al_2O_5(OH)_4\cdot(1-\chi)NH_4Cl\}$. The second mass loss (40%) occurred between 150 and 300 °C and corresponds to the departure of poral water. The third mass loss is situated between 450 and 600° and is ascribed to the de-hydroxylation of nacrite (~550 °C) leading to amorphous synthetic phase, commonly named metanacrite and characterized by a disordered polymerized silicon/aluminum framework (Jaafar et al., 2016). In the same line, calcination of nacrite-NH_4Cl nanohybrid around this temperature leads to its amorphization:

At the beginning of the de-hydroxylation ($T = 450$ °C), the chemical decomposition reaction of the nanohybrid per half unit cell can be expressed as follow.

$$Si_2Al_2O_5(OH)_4\cdot(1-\chi)NH_4Cl \rightarrow Si_2Al_2O_7\cdot(1-\chi)NH_4Cl + 2H_2O.$$

This loss is characterized by the removal of two structural water molecules. The nacrite-NH_4Cl nanohybrid is then converted to metanacrite-NH_4Cl nanohybrid as presented in Fig. 7 with the structural formula $\{Si_2Al_2O_7\cdot(1-\chi)NH_4Cl\}$.

Proceeding with the in-situ heat-treatment of the nanohybrid (at $T > 450$ °C) generates the increase of amorphicity and the evaporation of chlorine anions. This step was eventually accompanied by the evolution of the hydrogen halide which results from the following thermal hydrolysis (Gabor et al., 1986):

$$2SiO_2\cdot Al_2O_3 + (1-\chi)NH_4Cl \rightarrow 2SiO_2\cdot Al_2O_3\cdot\tfrac{(1-\chi)}{2}(NH_4)_2O + (1-\chi)HCl - \tfrac{(1-\chi)}{2}H_2O.$$

On the clay surface a liberated water molecule associates with Cl^- to form volatile HCl. The volatilization of HCl is responsible for thermal mass loss of the examined nanohybrid. This phenomenon causes the trapping of ammonium oxide "$(NH_4)_2O$" within the metanacrite matrix and the production of metanacrite-$(NH_4)_2O$ nanohybrid (Fig. 7) with a structural formula: $\{Si_2Al_2O_7\cdot\frac{(1-\chi)}{2}(NH_4)_2O\}$. Knowing that $\frac{(1-\chi)}{2}$ coefficient is equal to 0.47–0.5, we can simplify this chemical formula and express our metanacrite-$(NH_4)_2O$ nanohybrid by the following formula: $\{Si_2Al_2O_7\cdot\frac{1}{2}(NH_4)_2O\}$.

Hence, the thermal decomposition process estimates the water content of the nanohybrid and confirms the quantitative XRD analysis.

Table 4
Mass loss of the elaborated nacrite-NH_4Cl nanohybrid.

Nacrite-NH_4Cl nanohybrid	$\frac{\Delta m}{m}$	$-n$ H_2O per half unit-cell
Mass loss 1	0.73%	-1 H_2O
Mass loss 2	40.00%	-6 H_2O
Mass loss 3	09.59%	-2 H_2O
Total mass loss	50.32%	

3.4. Electrochemical study

3.4.1. Impedance analysis

Some complex impedance diagrams (Z'' vs Z') at various temperatures are given in Fig. 8. Examination of these curves illustrated the conducting behavior of the nanohybrid material. The evolution of $-Z'' = f(Z')$ curves revealed that the resistance diminishes as temperature increases. This phenomenon is attributed to a deformation (destruction) of some physical characteristics of the host clay material framework and to some chemical characteristics of NH_4Cl halide. The impedance diagrams for the nacrite-NH_4Cl nanohybrid are interpreted

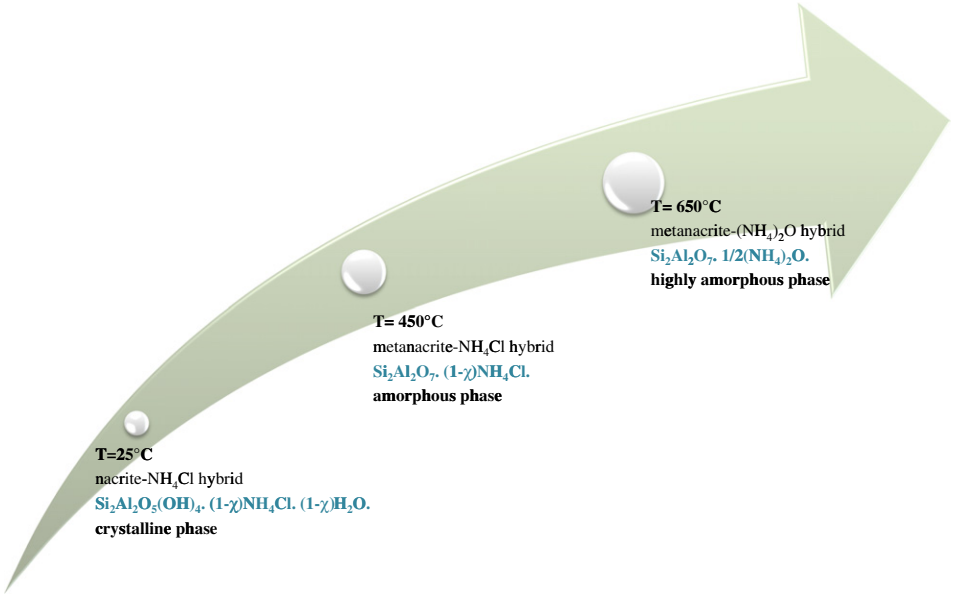

Fig. 7. Schematic representation of the thermal transformations of heat-treated nacrite-NH_4Cl nanohybrid from room temperature to 873 K.

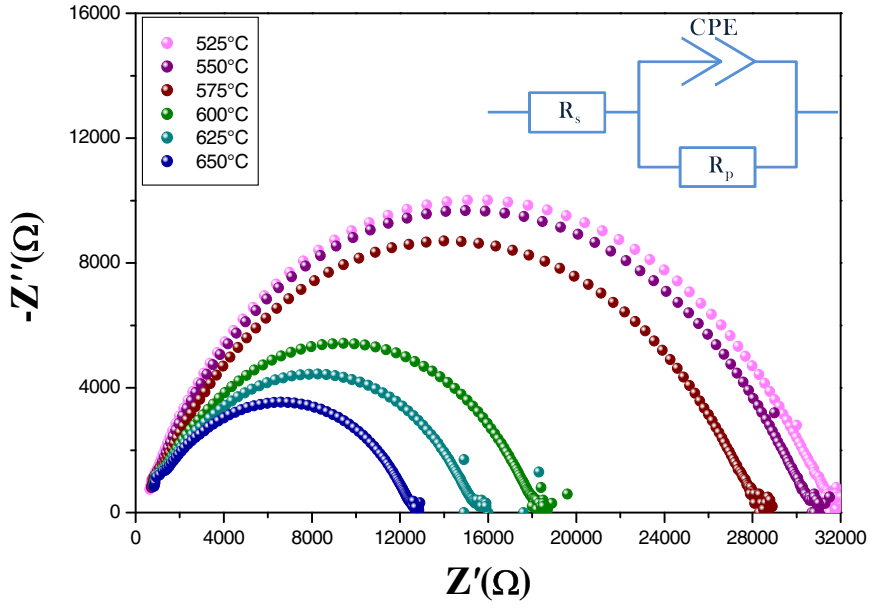

Fig. 8. Complex impedance diagrams of the nacrite-NH_4Cl nanohybrid over the temperature range 525–650 °C. The inset figure shows the equivalent circuit model of the compound.

using a fit procedure. In the temperature range 525–650 °C, the equivalent circuit that best matches the response of the nanohybrid is: R_s// (CPE, R_p), R_s is the grain resistance connected in series and R_p the grain resistance connected in parallel to an intuitive element, called capacity of the fractal interface (CPE) (Fig. 8). The (CPE) element accounts for the observed depression of semicircles and also the non-ideal electrode geometry. The impedance of this constant phase element is represented in Eq. (5):

$$Z_{CPE} = \frac{1}{Y_0(j\omega)^{\beta}} \tag{5}$$

where Y_0 is the admittance ($1/|Z|$) at $\omega = 1$ rad/s and β a value between 0 and 1.

3.4.2. Electrical conductivity

The temperature dependence of the dc conductivity was adjusted by the Mott's equation (Barsoukov and Macdonald, 2005):

$$\sigma_{dc} = \frac{\sigma_0}{T} \exp\left(\frac{-E_{a(dc)}}{k_B T}\right) \tag{6}$$

where $E_{a(dc)}$ is the activation energy for dc conductivity, k_B is the Boltzmann's constant and T the temperature in Kelvin, σ_0 is called the pre-exponential factor.

Table 5
ac and dc conductivity values of the nacrite-NH_4Cl nanohybrid.

Temperature region [°C]	σ_{dc} ($S \cdot m^{-1}$)	σ_{ac} ($S \cdot m^{-1}$)			
		$f = 100$ Hz	$f = 1$ MHz	$f = 5$ MHz	$f = 10$ MHz
425	$7.41 \cdot 10^{-6}$	$8.76 \cdot 10^{-6}$	$1.20 \cdot 10^{-3}$	$2.39 \cdot 10^{-3}$	$3.31 \cdot 10^{-3}$
450	$1.62 \cdot 10^{-5}$	$1.69 \cdot 10^{-5}$	$1.51 \cdot 10^{-3}$	$3.80 \cdot 10^{-3}$	$6.60 \cdot 10^{-3}$
475	$3.31 \cdot 10^{-5}$	$3.31 \cdot 10^{-5}$	$1.51 \cdot 10^{-3}$	$3.80 \cdot 10^{-3}$	$6.76 \cdot 10^{-3}$
500	$8.91 \cdot 10^{-5}$	$9.12 \cdot 10^{-5}$	$1.54 \cdot 10^{-3}$	$3.98 \cdot 10^{-3}$	$6.91 \cdot 10^{-3}$
525	$1.87 \cdot 10^{-4}$	$1.99 \cdot 10^{-4}$	$1.54 \cdot 10^{-3}$	$4.26 \cdot 10^{-3}$	$7.24 \cdot 10^{-3}$
550	$1.94 \cdot 10^{-4}$	$1.94 \cdot 10^{-4}$	$1.62 \cdot 10^{-3}$	$4.78 \cdot 10^{-3}$	$7.94 \cdot 10^{-3}$
575	$1.99 \cdot 10^{-4}$	$2.13 \cdot 10^{-4}$	$1.65 \cdot 10^{-3}$	$5.24 \cdot 10^{-3}$	$8.91 \cdot 10^{-3}$
600	$3.88 \cdot 10^{-4}$	$3.46 \cdot 10^{-4}$	$1.73 \cdot 10^{-3}$	$5.37 \cdot 10^{-3}$	$9.12 \cdot 10^{-3}$
625	$3.80 \cdot 10^{-4}$	$3.98 \cdot 10^{-4}$	$1.86 \cdot 10^{-3}$	$5.49 \cdot 10^{-3}$	$9.26 \cdot 10^{-3}$
650	$4.89 \cdot 10^{-4}$	$4.78 \cdot 10^{-4}$	$4.67 \cdot 10^{-3}$	$9.12 \cdot 10^{-3}$	$3.80 \cdot 10^{-2}$

The σ_{dc} conductivity of nacrite-NH_4Cl nanohybrid increases from ($7.41 \cdot 10^{-6}$ $S \cdot m^{-1}$) at 425 °C to the ($4.89 \cdot 10^{-4}$ $S \cdot m^{-1}$) at 650 °C (Table 5). The logarithmic variation of the dc conductivity shows two slopes (Fig. 9), which correspond to two activation energies 0.64 eV and 1.61 eV, respectively below and above 525 °C (Fig. 9). These values suggest an ionic conduction process. Moreover, the break in the curve (Fig. 9), attributed to the phase transition from crystalline to amorphous state in the TGA measurement (Fig. 6), indicates that the ionic conductivity is strongly enhanced by the amorphization of the nanohybrid.

The temperature dependence of the ac conductivity was determined using the Arrhenius expression (Hummel, 2011):

$$\sigma_{ac} = \sigma_0 \exp\left(\frac{-E_{a(ac)}}{k_B T}\right) \tag{7}$$

As listed in (Table 5), σ_{ac} increases from ($3.31 \cdot 10^{-3}$ $S.m^{-1}$) at 500 °C to ($3.80 \cdot 10^{-2}$ $S \cdot m^{-1}$) at 650 °C measurements at high frequencies (10 MHz). This increase is related to that of the number of free ions in the nanohybrid matrix in terms of temperature and designates that

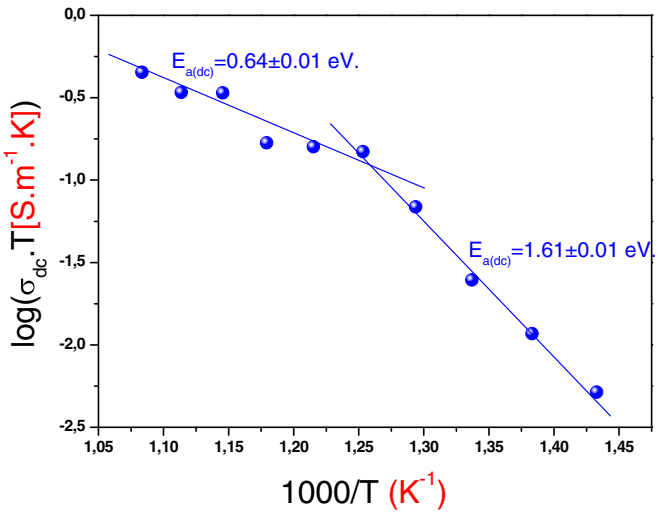

Fig. 9. $\log(\sigma_{dc} \cdot T) = f(1000/T)$ of nacrite-NH_4Cl nanohybrid material.

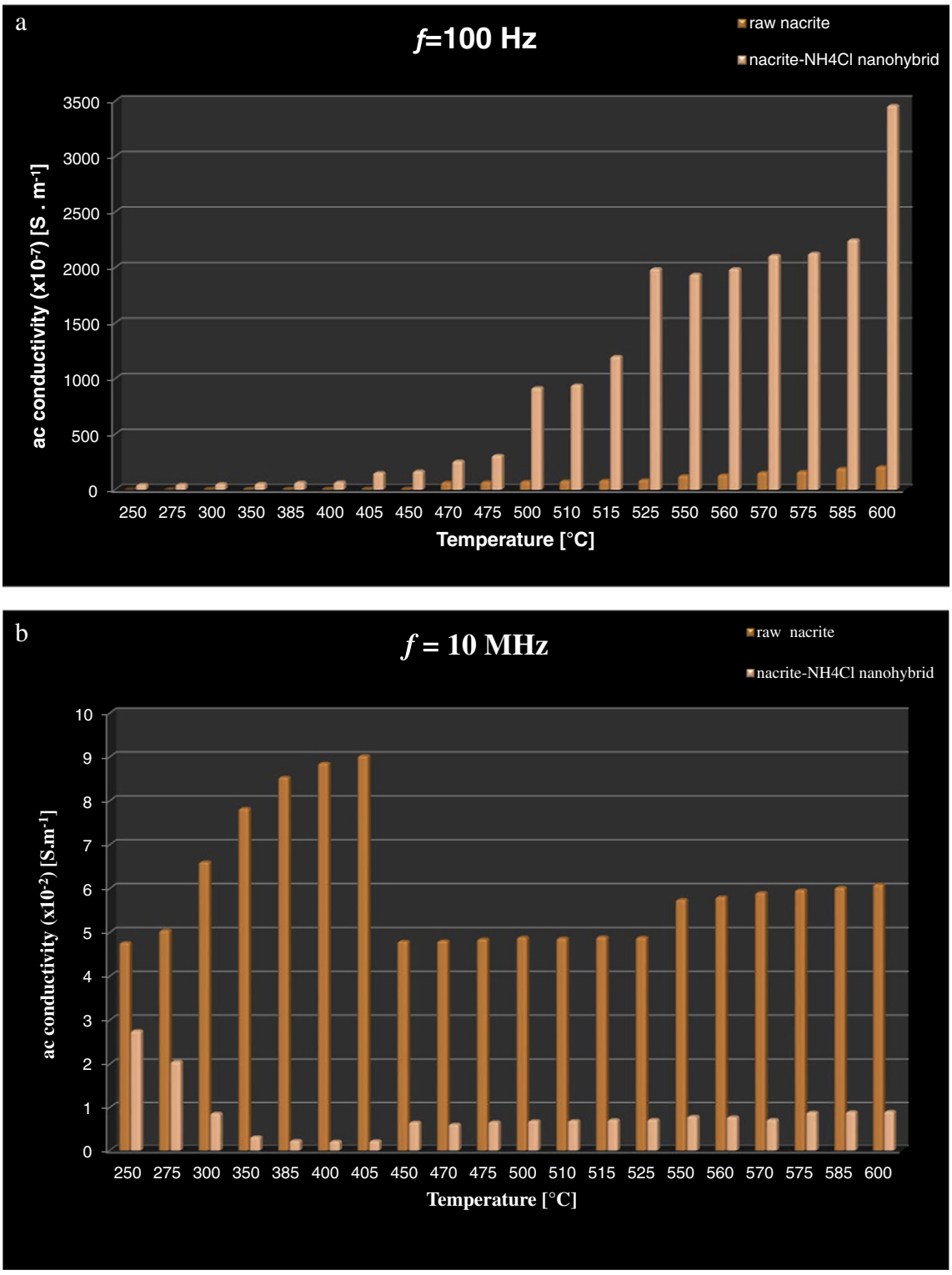

Fig. 10. a. Comparison between ac conductivity of raw nacrite and nacrite-NH_4Cl nanohybrid at a fixed frequency $f = 100$ Hz and different temperatures. b. Comparison between ac conductivity of raw nacrite and nacrite-NH_4Cl nanohybrid at a fixed frequency $f = 10$ MHz and different temperatures.

the ionic transport mechanism can be interpreted by the thermally activated hopping process.

According to these experimental results, a strong jump in the conductivity is detected characterizing a superionic conduction phase transition indicating that the disordered nanohybrid bears easier motion than the ordered one. To conclude, the contribution of disorder and defects in the nanohybrid framework are responsible for the motion of charge carriers; this result is consistent with the previous publication of Kumar and Yashonath (2006).

In the following part, we investigate the charge carriers responsible for conduction in our nanohybrid around the de-hydroxylation temperature:

Before de-hydroxylation, nacrite-NH_4Cl nanohybrid material displayed a well-packed structure according to the XRD analysis.

Furthermore, due to the strong interactions between the nacrite host matrix and the intercalated species as determined by IR spectroscopy, the structural O^{2-}, H^+ and OH^- ions of the fairly rigid aluminosilicate framework are localized around their equilibrium sites, i.e., they cannot escape from their lattice sites. Besides, H^+ and OH^- ions of the intercalated water molecules are eliminated during the dehydration starting from 100 °C as shown by TGA. Knowing that, Cl^- anion appears to be rather less mobile than the NH_4^+ cation due to its great ionic radius (Kumar and Yashonath, 2006), the NH_4^+ is the predominant current carrier in the nacrite-NH_4Cl nanohybrid at low temperatures.

During de-hydroxylation, in the temperature range between 450 and 650 °C, nacrite-NH_4Cl nanohybrid converts to metanacrite-NH_4Cl nanohybrid and then to metanacrite-$(NH_4)_2O$ nanohybrid containing large amount of amorphous silico-aluminates; therefore disorder and/or defects arise. In this temperature range, de-hydroxylation is accompanied by removal of the inner-surface hydroxyls and the inner hydroxyls from the nacrite framework. Therefore, OH^- and H^+ ions did not contribute to the ionic conduction process. Besides, a new Si—O—Al bond is created during de-hydroxylation, which prevents the contribution of O^{2-} anions to the transport mechanism. Hence, the high ionic conductivity of $\{Si_2Al_2O_7\cdot(1-\chi)NH_4Cl\}$ nanohybrid (Fig. 7) is reasonable since the amorphous structure is so suited for easy motion of NH_4^+ ions. However, $\{Si_2Al_2O_7\cdot\frac{1}{2}(NH_4)_2O\}$ nanohybrid exhibited higher conductivity as reported in Fig. 7. This improvement in conductivity may be explained by the presence of $(NH_4)_2O$ content oxide into the highly amorphous matrix through which the mobile ions migrate. This oxide increases the number of non-bridging oxygen than bridging oxygen (NBOs) in the amorphous matrix (Altaf and Chaudhry, 2010; Veeranna Gowda et al., 2013). Consequently, the enhanced conductivity is associated with the increase in the non-bridging oxygen (NBOs) and the resulting improved NH_4^+ ion mobility (Kim et al., 2012).

Finally, NH_4^+ is the common current carrier via hopping from one site to the next for both amorphous "metanacrite-NH_4Cl hybrid" and highly amorphous "metanacrite-$(NH_4)_2O$ nanohybrid". This implies that the conductivity is preferentially affected by the amorphicity of the metanacrite framework through which mobile ammonium ions may hop.

Comparison between the electrochemical features of the elaborated nacrite-NH_4Cl nanohybrid and raw nacrite reveals that, at low frequency ($f = 100$ Hz) (Fig. 10a), the ac conductivity of nacrite-NH_4Cl nanohybrid arises remarkably in terms of temperature, and for a fixed temperature, the ac conductivity of nacrite-NH_4Cl nanohybrid is greater than the ac conductivity of raw nacrite. In the meanwhile, at high frequency ($f = 10$ MHz) (Fig. 10b), the ac conductivity varies randomly when the temperature increases, and for a fixed temperature, the ac conductivity of raw nacrite is greater than that nacrite-NH_4Cl nanohybrid.

In other words, at low frequency, the ac conductivity is enhanced by the incorporation of ammonium chloride. However, at high frequency, the ac conductivity is not sensitive to the addition of salt. In conclusion, the intercalation of ammonium cation in the interlamellar space of nacrite caused significant changes in its physical properties. The electrical properties of the resulting nanohybrid are different from those of the starting material; this is due to multiple structural perturbations at the surfaces and interfaces during the incorporation of the ions.

4. Concluding remark

This study has been achieved in order to accomplish an effective intercalation process of NH_4Cl salt in the interlamellar space of nacrite and to understand the resulting changes of the structural, thermal and electrical properties of the elaborated nanohybrid. Accurate XRD characterization and simulation showed that the basal distance increased from 0.72 to 1.03 nm and that the salt is inserted successfully into the interlayer space of nacrite as follows: one NH_4^+ cation located at $z = 0.81 \pm 0.01$ nm, one Cl^- anion located at $z = 0.66 \pm 0.01$ nm and one water molecule situated at $z = 0.70 \pm 0.01$ nm sandwiched between the cation and the anion. IR spectroscopy allowed the study of interactions between the silicate network and the inserted species. The thermal properties of the nanohybrid confirmed the intercalation of the hydrated salt in the interlamellar space of nacrite. Consequently, nacrite is an excellent clay mineral host matrix for further intercalation reactions. Electrical properties have been offered to monitor the effect of the cation on the conduction process of the nacrite-NH_4Cl nanohybrid. Finally, the elaborated nanohybrid seems to be interesting since it exhibits high conductivity at high temperature. Thus, it belongs to the family of superionic conductors which are of great interest because of their potential use in various electrochemical power sources.

Acknowledgements

Dr. Nouha Jaafar acknowledges Professor Hafsia Ben Rhaiem, Unity of Research of Physics of Lamellar Materials and Hybrid Nano-Materials, University of Carthage, Tunisia for her main contribution in the proof reading of the paper and for language refinement.

References

Altaf, M., Chaudhry, M.A., 2010. Physical properties of lithium containing cadmium phosphate glasses. J. Mod. Phys. 1, 201–205.
Barsoukov, E., Macdonald, J.R., 2005. Impedance Spectroscopy: Theory, Experiment, and Applications. second ed. Wiley, Hoboken (ISBN: 978-0-471-64749-2).
Ben Haj Amara, A., 1997. X-ray diffraction, infrared and TGA/DTG analysis of hydrated nacrite. Clay Miner. 32, 463–470.
Ben Haj Amara, A., Plançon, A., Ben Brahim, J., Ben Rhaiem, H., 1998. XRD study of the stacking mode of natural and hydrated nacrite. Mater. Sci. Forum 278-281, 809–813.
Ben Haj Amara, A., Ben Rhaiem, H., Plançon, A., 2000. Structural evolution of nacrite as a function of the nature of the intercalated organic molecules. J. Appl. Crystallogr. 33, 1351–1359. http://dx.doi.org/10.1107/S0021889800011730.
Ben Rhaiem, H., Tessier, D., Ben Haj Amara, A., 2000. Mineralogy of the <2 μm fraction of three mixed-layer clays from southern and central Tunisia. Clay Miner. 35, 375–381. http://dx.doi.org/10.1180/000985500546846.
Bergaya, F., Lagaly, G., 2006. General introduction: clays, clay minerals, and clay science. In: Bergaya, F., Theng, B.K.G., Lagaly, G. (Eds.), Handbook of Clay Science: Developments in Clay Science Vol. 1. Elsevier, Amsterdam, pp. 1–18.
Brigatti, M.F., Galan, E., Theng, B.K.G., 2013. Structure and mineralogy of clay minerals. In: Bergaya, F., Lagaly, G. (Eds.), Handbook of Clay Science: Developments in Clay SciencePart A: Fundamentals Vol. 5. Elsevier, Amsterdam, pp. 21–82.
Brunet, E., Colón, J.L., Clearfield, A., 2015. Tailored Organic-Inorganic Materials. Wiley.
Drits, V.A., Tchoubar, C., 1990. The modelization method in the determination of the structural characteristics of some layer silicates: internal structure of the layers, nature and distribution of stacking faults. X-ray Diffraction by Disordered Lamellar Structures. Springer-Verlag, Berlin, pp. 233–303.
Fernandes, F.M., Baradari, H., Sanchez, C., 2014. Integrative strategies to hybrid lamellar compounds: an integration challenge. Appl. Clay Sci. 100, 2–21.
Frost, R.L., Kristof, J., Mako, E., Kloprogge, J.T., 2000. Modification of the hydroxyl surface in potassium-acetate-intercalated kaolinite between 25 and 300 °C. Langmuir 16, 7421–7428. http://dx.doi.org/10.1021/la9915318.
Gabor, M., Poeppl, L., Koeros, E., 1986. Effect of ambient atmosphere on solid state reaction of kaolin-salt mixtures. Clay Clay Miner. 34, 529–533. http://dx.doi.org/10.1346/CCMN.1986.0340505.
Garrett, W.G., Walker, G.F., 1959. The cation-exchange capacity of hydrated halloysite and the formation of halloysite-salt complexes. Clay Miner. Bull. 4, 75–80. http://dx.doi.org/10.1180/claymin.1959.004.22.02.
Hummel, R.E., 2011. Electronic Properties of Materials. Springer.
Jaafar, N., Ben Rhaiem, H., Ben Haj Amara, A., 2014. Synthesis, characterization and applications of a new nanohybrid composite: nacrite/$MgCl_2\cdot 6H_2O$/ethanol. International Conference on Composite Materials and Renewable Energy Applications (ICCMREA), Sousse, 22–24 January 2014a, pp. 1–6.
Jaafar, N., Naamen, S., Ben Rhaiem, H., Ben Haj Amara, A., 2015. Functionalization and structural characterization of a novel nacrite-LiCl nanohybrid material. Am. J. Anal. Chem. 6, 202–215.
Jaafar, N., Ben Rhaiem, H., Ben Haj Amara, A., 2016. Structural and electrochemical properties of cementitious and hybrid materials based on nacrite. In: Do Nascimento, G.M. (Ed.), Clays, Clay Minerals and Ceramic Materials Based on Clay Minerals. InTech http://dx.doi.org/10.5772/61594 (ISBN: 978-953-51-4597-4).
Kim, Y.H., Yoon, M.Y., Lee, E.J., Hwang, H.J., 2012. Effect of SiO_2/B_2O_3 ratio on Li ion conductivity of a $Li_2OB_2O_3$-SiO_2 glass electrolyte. J. Ceram. Process. Res. 13, 37–41.
Kumar, P.P., Yashonath, S., 2006. Ionic conduction in the solid state. J. Chem. Sci. 118, 135–154.
Lagaly, G., Ogawa, M., Dékany, I., 2006. Clay mineral organic interactions. In: Bergaya, F., Theng, B.K.G., Lagaly, G. (Eds.), Handbook of Clay Science: Developments in Clay Science Vol. 1. Elsevier, Amsterdam, pp. 309–378.

Naamen, S., Ben Rhaiem, H., Karmous, M.S., Ben Haj Amara, A., 2004. XRD study of the stacking mode of the nacrite/alkali halides complexes. Mater. Struct. 11.
Petit, S., Righi, D., Madejova, J., 2006. Infrared spectroscopy of NH_4^+-bearing and saturated clay minerals: a review of the study of layer charge. Appl. Clay Sci. 34, 22–30.
Shoval, S., Yariv, S., Michaelian, K.H., Boudeulle, M., Panczer, G., 2001. LO and TO crystal modes of the hydroxyl stretching vibrations in micro-Raman and infrared spectra of nacrite. Opt. Mater. 16, 311–318.
Taser, M., Kuçukcelebi, H., Armagan, N., Guler, G., 1997. Use of R factors in the study of the structural defects in phyllosilicates by X-ray powder diffraction. J. Appl. Crystallogr. 30, 55–58.
Veeranna Gowda, V.C., Narayana Reddy, C., Rao, K.J., 2013. A new approach for understanding ion transport in glasses; example of complex alkali diborate glasses containing lead, bismuth and tellurium oxides. Bull. Mater. Sci. 36, 71–85.
Wada, K., 1959. An interlayer complex of halloysite with ammonium chloride. Am. Mineral. 44, 1237–1247.
Wypych, F., Satyanarayana, K.G., 2004. Clay Surfaces, Fundamentals and Applications. Academic Press/Elsevier, Waltham/Amsterdam.
Yariv, S., Lapides, I., Michaelian, K.H., Lahav, N., 1999. Thermal intercalation of alkali halides into kaolinite. J. Therm. Anal. Calorim. 56, 865–884. http://dx.doi.org/10.1023/A:1010187029708.
Zhang, J., Cheng, H., Liu, Q., He, J., Frost, R.L., 2011. Mid-infrared and near-infrared spectroscopic study of kaolinite- potassium acetate intercalation complex. J. Mol. Struct. 994, 55–60.
Zhou, C.H., Keeling, J., 2013. Fundamental and applied research on clay minerals: from climate and environment to nanotechnology. Appl. Clay Sci. 74, 3–9.
Zhou, C.H., Zhao, L.Z., Wang, A.Q., Chen, T.H., He, H.P., 2016. Current fundamental and applied research into clay minerals in China. Appl. Clay Sci. 119, 3–7.
Zhu, R., Sanchez, C., Bergaya, F., 2014. Special issue advances in applied clay science intercalated nanomaterials: from functional clays to advanced hybrid lamellar compounds. Appl. Clay Sci. 100, 1. http://dx.doi.org/10.1016/j.clay.2014.08.008.